BMC Genomics

RESEARCH

Open Access

MicroRNA expression dynamics in mouse liver at different stages of *Echinococcus multilocularis* infection

Ying Chen[1†], Hai-Jun Gao[2†], Chen Li[1,2†], Xiao-Jin Mo[2,3], Gui-Rong Zheng[1], Jun Xie[1], Jie Gao[1], Bolor Bold[2,5], Zheng Feng[2], Ting Zhang[1,2,3*] and Wei Hu[1,2,4*]

Abstract

Background Alveolar echinococcosis (AE) is a globally widespread zoonotic disease caused by the larval stage of the tapeworm *Echinococcus multilocularis*, posing a high fatality rate and poor prognosis if not properly managed. Currently, effective vaccines or drugs for echinococcosis remain elusive. MicroRNAs (miRNAs) play crucial roles in various biological processes and are closely linked with parasite infection and pathogenicity. To date, there is limited knowledge about host miRNA profiles in *E. multilocularis* infection at different stages. Hence, exploring host miRNA expression patterns at different infection stages is vital for understanding miRNA transcriptional regulation mechanisms.

Methods This study employs small RNA sequencing to depict the temporal dynamics of miRNAs in mice liver at 40, 80, and 120 dpi with *E. multilocularis*. Additionally, Short Time-series Expression Miner, Gene ontology, KEGG pathway, and miRNA-target gene-pathway network analysis were conducted to elucidate each miRNA's changing trends, focusing on the hub miRNAs during infection. Subsequently, miRNA altering patterns at 40, 80, and 120 dpi were confirmed via quantitative real-time PCR.

Results The findings reveal time-dependent miRNA expression profiles, categorized into three distinct patterns specific to early, middle, and late infection stages. Overall, 61 miRNAs were stage-differentially expressed in the livers of infected mice compared to uninfected mice, with 29 miRNAs up-regulated and 32 miRNAs down-regulated. Notably, in the early phase, 23 miRNAs showed differential expression, with 18 up-regulated and 5 down-regulated ($|\log_2 FC| > 1$, $P < 0.05$). Moreover, genes regulated during this phase primarily involved in Th17 cell differentiation, AMPK signaling pathway, and Calcium signaling pathway. Subsequently, during the middle infection stage, a total of 16 miRNAs exhibited differential expression, with 8 up-regulated and 8 down-regulated ($|\log_2 FC| > 1$, $P < 0.05$). These miRNAs are involved in prolactin signaling pathway, aldosterone synthesis secretion, and Cushing's syndrome. In the

†Ying Chen, Hai-Jun Gao and Chen Li contributed equally to this work.

*Correspondence:
Ting Zhang
zhangting@nipd.chinacdc.cn
Wei Hu
huw@imu.edu.cn

Full list of author information is available at the end of the article

late infection stage, 22 differentially expressed miRNAs were identified, with 3 up-regulated and 19 down-regulated ($|\log_2 FC| > 1$, $P < 0.05$). Furthermore, the identified target genes primarily participated in ECM-receptor interaction, TGF-β signaling pathway, and human papillomavirus infection pathway. Also, through network interaction analysis, it was speculated that *Src*, *Jag1*, and *Mapk1* exhibited the most hub signaling genes during the early, middle, and late infection stages, respectively, while the *Srf* was dynamically expressed hub signaling gene throughout the whole infection stage. As the disease progresses, several hub networks have been identified around target genes, including the mmu-miR-1247-5p-*Src*-Rap1 signaling pathway, mmu-miR-149-5p-*Jag1*-Notch signaling pathway, mmu-miR-299a-5p-*Mapk1*-human papillomavirus infection pathway in the early, middle and late stages, respectively. Additionally, the mmu-miR-122-3p-*Srf*-MAPK signaling pathway was predicted to be the hub network in the whole infection stage.

Conclusions Overall, our investigation elucidates the temporal dynamic changes in host miRNAs and their potential target genes at the early, middle and late stages of *E. multilocularis* infection, which allows us to understand the roles of miRNAs in host-parasite interactions throughout infection and provides a reference for further studies of molecular pathogenesis and new drug or vaccine targets for control of AE.

Keywords *Echinococcus multilocularis*, MiRNA, RNA sequencing, Echinococcosis

Author summary

Alveolar echinococcosis (AE), a chronic parasitic disease known as "worm cancer" poses a significant burden on public health and economic development due to its high disability and mortality rates. The lack of early diagnostic markers and effective therapeutic interventions further exacerbates the impact of this disease. In this study, we analysed the dynamic profiles of miRNA in the liver of mice infected with *E. multilocularis*, identifying a batch of hub differentially expressed miRNAs, putative target genes, and enriched pathways across the early, middle and late infection stages. These markers reflect host regulation associated with AE progression, gradually transitioning from initial immune regulation to reprogramming of metabolism and ultimately forming the liver fibrosis pathology. Our findings will be essential for developing diagnostic markers or identifying targets for AE vaccines and drugs in the future.

Introduction

Alveolar echinococcosis (AE) stands as a significant zoonotic parasitic affliction, arising from the larval stage (metacestode) of *Echinococcus multilocularis* (*E. multilocularis*), posing considerable pathogenicity and high fatality rates [1]. If left untreated, AE is highly fatal with a mortality of over 90% [2]. Its ramifications in global human health and animal husbandry are severe. According to World Health Organization (WHO) data, there are approximately 18,200 annual AE infections worldwide, with an estimated 6.66 million disabled life years (DALYs) attributed to AE globally [3]. AE is among the 17 neglected diseases targeted for control or elimination by WHO by 2050 [4]. Presently, there are no viable alternative drugs, vaccines, or diagnostic kits for echinococcosis, underscoring the pressing need for discovery of novel effective treatment strategies and diagnostic targets via genomic, transcriptomic, and other high-throughput screening methodologies.

Echinococcus spp. are zoonotic parasites, the definitive hosts are carnivorous predators - dogs, wolves, foxes, and the intermediate hosts are usually sheep, goats, cattle, and rodents, which are infected by ingestion of eggs. Humans are also could be accidentally infected. After infected, *E. multilocularis* metacestodes predominantly located in the liver (in 99% of cases) [5, 6]. Oncosphere larvae are released from the egg and passed through the portal to reach liver, where they reside and develop into larvae (metacestodes) [7]. Clinically, the infection is always chronic and asymptomatic, and the disease progression of AE usually results from a continuous and complex interaction between the parasite and the host [7]. AE pathology involves infiltration of a large number of inflammatory cells around the parasitic periphery and further development of granulomas or liver fibrosis, which is mainly orchestrated by the response pattern of cytokines and immune or non-immune cells [8, 9]. Thus, the host liver may exhibit different degrees of pathological changes that are prolonged with AE progression [10].

Previously, we found that persistent *E. multilocularis* infection in gerbils induced elevated deposition of collagen fibers in the liver, and the highest level of CoI1a1 and α-SMA was observed 6 to 8 months post-infection [11]. Other studies have shown that in the early stage of infection, the immune balance between humans and *Echinococcus* is disrupted, and the development of fibrosis is at stake [12]. In the middle stage of infection, invasive parasitic lesions and progressive hepatomegaly may be associated with all types of cytokines and impairment of the immune system [10]. In the later stage of the disease, massive expansion and infiltration of metacestodes in the liver of intermediate hosts induce liver fibrosis and necrosis, which may even progress to organ failure [13].

The observed pathological alterations in the host liver that occur throughout the progression of infection may be attributed to the temporal regulation of genes [14], cytokines [15], or proteins [16]. However, little is known on miRNA regulation in the liver during *E. multilocularis* infection.

MiRNAs are powerful genetic regulators, playing significant role in posttranscriptional regulation of numerous cellular signaling pathways [17]. The role of miRNAs in the regulation of host-parasite interactions has attracted significant interest [18], and miRNAs have emerged as potential targets for vaccine, drug development and diagnostic purposes in parasitic disease [19]. During the initial phase of *E. multilocularis* protoscolex infection, the expression of miRNAs in abdominal macrophages [20] and the liver of mice [21] is known to be involved primarily in the regulation of the host immune response and liver cell necrosis and fibrosis, respectively. However, the dynamic changes in more advanced stages of infection remain unclear. A study investigated the dynamic circRNA profiles in liver cells of mice infected with *E. multilocularis* at 2 and 3 months, yet the miRNA profiles are still unexplored [22]. Therefore, further investigation into the role of miRNAs in AE pathogenesis is warranted.

In this study, an infection model was established by in situ surgical intrahepatic implantation to reproduce the natural onset and development of AE in murine mice [23]. Using this model, the temporal dynamics of miRNAs in the livers of *E. multilocularis*-infected mice were investigated via next-generation sequencing (NGS), and the significant dynamic variations in miRNAs were validated by qRT-PCR. In addition, systematic bioinformatics analyses integrating functional annotation of miRNAs, construction of miRNA-target gene-pathway regulatory networks, and Short Time-series Expression Miner (STEM)-based temporal clustering were conducted to delineate the multi-dimensional mechanisms underlying miRNA-mediated regulation during AE progression.

Materials and methods

Animal model and parasite infection

Kunming mice (8 weeks, female, weight 20±2 g) were purchased from Shanghai Jiesijie Experimental Animal Co., LTD and kept under specific pathogen-free laboratory conditions and fed a rodent diet ad libitum. Female-specific pathogen-free (SPF) mice ($n = 20$) were stratified into four groups: an uninfected control group ($n = 5$) and three *E. multilocularis*-infected groups at 40 dpi (early stage, $n = 5$), 80 dpi (middle stage, $n = 5$), and 120 dpi (late stage, $n = 5$). The control group remained uninfected, and the other three groups were infected with *E. multilocularis* protoscolices (1500 PSCs/mouse) by in situ surgical intrahepatic implantation that mimics naturally infected livers, according to the parasite load. The PSCs (Chinese mainland isolate, Qinghai population) used in this study were obtained from our laboratory infected jirds as described previously [23]. All animal infections were performed under SPF laboratory conditions.

Tissue sampling and histopathological examination of the parasitic lesions and surrounding liver parenchyma

The experimental mice were first subjected to isoflurane-induced anesthesia. Subsequently, blood samples were collected using the enucleating eyeball method. These blood samples were then centrifuged at 3000 rpm and 4 °C for 15 min to separate them into serum samples. A fully automated biochemical analyzer (BS-240VET, China) was employed to assess liver-related biochemical indicators (ALT, AST) in mice sera.

After blood collection, the mice were euthanized through cervical dislocation and dissected to remove their livers. For miRNA sequencing, three pieces of liver tissue, totaling 0.1 g per mouse, were collected from a site 0.5 cm away from the metacestode cyst to minimize potential contamination. The tissues were immediately frozen in liquid nitrogen and stored for subsequent analysis. For pathological analysis, the mouse livers were fixed with 4% paraformaldehyde, embedded in paraffin, sectioned, stained, and subjected to histopathological (H&E) analyses. The extent of collagen deposition in the liver tissue at various infection time points was evaluated using Sirius red staining and Masson staining methods. Histopathological staining results were analyzed through software *Image J Fiji* (https://imagej.net/Fiji).

Small RNA extraction and library construction

RNA purification, reverse transcription, library construction, and sequencing were conducted at Mingma Technologist in Shanghai. Total RNA was extracted from frozen livers using the QIAseqTM miRNA Library Kit (Qiagen) following the manufacturer's protocol, and its concentration was quantified with a Nanodrop 2000 (Thermo Fisher Scientific Inc., USA). Approximately 50 ng of eluted total RNA was utilized for ligating 3' adapters, followed by 5' adapters ligation. First-strand cDNA was synthesized using reverse transcriptase and RT primers containing 12 bp Unique Molecular Indices, followed by second-strand cDNA synthesis. Library amplification was achieved using a universal forward primer paired with reverse primers assigning a sample index. Following amplification, the miRNA library was cleaned-up using streamlined magnetic bead-based method. Subsequently, the concentration of the resulting sequencing libraries was quantified using a Qubit 2.0 fluorometer dsDNA HS Assay (Thermo Fisher Scientific), while the size distribution was analyzed using Agilent Bio Analyzer

(Agilent, USA). Sequencing was conducted on Illumina Novaseq 6000 according to Illumina-provided protocols for 2 × 150 paired-end sequencing. The configuration typically results in a high Q30 ratio (the proportion of bases with a Phred quality score > 30), which ensures the higher accuracy and reliability of the sequencing data [24, 25].

The basic reads underwent base calling to generate sequence data, also known as raw data/reads. To preprocess the raw data, low-quality reads containing poly (A) sequences and adapter contaminants were initially filtered out. Reads shorter than 15 nt or longer than 41 nt were also excluded to acquire clean reads. This step removed precursor miRNAs (pre-miRNAs), the nonfunctional immature transcripts, thereby restricting downstream analyses to mature miRNAs as the focus of this investigation.

To classify and annotate miRNAs in the sequencing data, the CleanReads were sequentially aligned against the Rfam database [26], cDNA sequences, the species-specific repeat sequence library [27], and the miRBase database (http://www.mirbase.org/) [28] for miRNA identification. Subsequently, the expression patterns of the identified known miRNAs at different infection stages. Following this, novel miRNAs were predicted using mirDeep2 [29]. Additionally, *Echinococcus*-derived miRNAs were identified through alignment of small RNA sequencing reads to the mature miRNA sequences in the MirGeneDB database (V2.1, https://mirgenedb.org/) using Bowtie 1 with parameters allowing up to three mismatches in the seed region (-v 3) [30, 31].

Identification of miRNA expression in the liver during the course of *E. multilocularis* infection

Differentially expressed miRNAs were identified with the following criteria: $|\log_2 FC| > 1$, adjusted $P < 0.05$, and an average normalized count ≥ 2 across samples. The DESeq2 package in R was used for differential miRNA screening in biological replicates, while the DESeq formula was used to calculate differences without biological replicates [32]. Volcano plots and heatmaps were used to visualize the significantly differentially expressed miRNAs in each group.

Prediction and functional annotation of miRNA target genes

The target genes of differentially expressed miRNAs were predicted by the software miRanda (www.microrna.org) with parameter settings of S ≥ 150, ΔG ≤ −30 kcal/mol and strict 5' seed pairing. The miRNA potential target genes were then selected for KEGG and GO analyses. Gene Ontology (GO) annotation and enrichment analyses were performed using Blast2GO (http://www.geneontology.org/) and GO-Term Finder (https://www.yeastgenome.org/goTermFinder). Up/down regulated transcripts (fold change ≥ 2) were examined by using an online Venn diagram tool (http://bioinfogp.cnb.csic.es/tools/venny/index.html) and gene function was annotated on the KEGG Automatic Annotation Server (KAAS).

STEM analysis and qRT-PCR validation of miRNAs

To analyze the trend of miRNA expression profiling across different infection stages, STEM analysis software (http://www.cs.cmu.edu/~jernst/stem) was employed. For validation of miRNA expression over infection stages, stem-loop real time qPCR was used. Primers were designed according to Yoann et al. [33], as shown in the Supplementary Table 1. One nanogram of RNA was reverse transcribed into cDNA using the stem-loop method. U6 was chosen as the internal reference gene, following the manufacturer's protocols (TAKARA: Cat. No. 638313). Each qRT-PCR reaction contained 12.5 µL of SYBR Green Master mix (TAKARA: RR820A) and was performed on a BioRad CFX96 Touch system with the following procedure: pre-denaturation at 95 °C for 5 min, followed by 40 cycles of 95 °C for 10 s and 60 °C for 30 s. Each sample was run in triplicate, and the expression levels were calculated using the $2^{-\Delta\Delta Ct}$ method [34].

Interaction network analysis of miRNA-target gene-pathway

Dynamic interaction networks of differentially expressed miRNAs and their putative target gene-associated pathways across three distinct temporal phases (early, middle, and late stages) were constructed using Cytoscape software (v3.8.2) [35]. Hub genes were computationally prioritized using the Bottleneck algorithm within the CytoHubba plugin, and the top 20 scored genes by betweenness centrality were defined as candidate hubs, followed by Cytoscape-based visualization [36].

Statistical analysis

The data were analyzed with SPSS 22.0 (IBM, Chicago IL, USA) and GraphPad Prism v6 (GraphPad Software, Inc., San Diego, USA) software. Principal component analysis (PCA, https://cloud.oebiotech.com) was used to visualize the similarities and variations between samples. Student's t-test was used to determine significant differences between two groups, and one-way ANOVA was used to determine significant differences among three or more groups. $|\log_2 FC| > 1$ and $P < 0.05$ was considered statistically significant.

Results

Hepatic injury induced by *E. multilocularis*

At 40 dpi, visible lesions (approximately < 1.0 cm) were evident and growing in the mice livers (Fig. 1). Pathological analysis was conducted to investigate the liver damage during the chronic infection. H&E staining showed

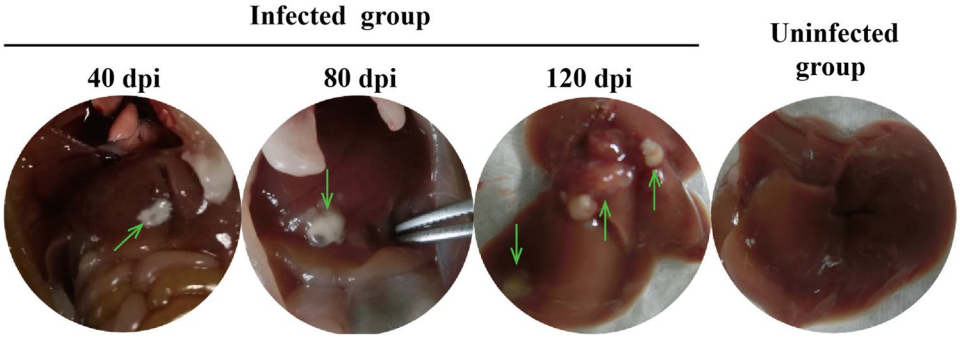

Fig. 1 *E. multilocularis* metacestode in mice at different infection stages. Note: Green arrow indicates the metacestode

that after 40 dpi, inflammatory cell infiltration appeared in the mice liver tissue (Fig. 2A). At the middle stage of infection (80 dpi), inflammatory cell infiltration worsened (Fig. 2A). At the late stage (120 dpi), fibrous bridges formed between hepatocytes, accompanied by a distinct inflammatory cell band surrounding the lesion and widespread necrotic foci throughout the hepatic parenchyma (Fig. 2A). At the same time, the infected group exhibited distinct metacestode lesions in comparison to the uninfected group, with the size of these lesions progressively increasing over the infection time (Fig. 2). At 40 dpi, masson's trichrome staining revealed punctate necrosis and peripheral inflammatory cell rim were identified, in contrast to the uninfected controls (Fig. 2B). By 80 dpi, a significant elevation in collagen deposition was observed (Fig. 2B). However, at 120 dpi, the liver lobule structure was compromised, resulting in indistinct outline and hardened liver texture (Fig. 2B). Masson's trichrome staining revealed distinct metacestode lesions at both the middle and late stages of infection, which consistent with the observations from H&E staining (Fig. 2B). Sirius red staining demonstrated that collagen deposition is positively correlated with the duration of infection stage (Fig. 2C). Quantitative analysis showed the area of positive Masson blue staining increased from 3.0 to 3.1% ($P > 0.05$), 8.8% ($P < 0.001$), and 18.0% ($P < 0.0001$) during the early, middle, and late stages of infection, respectively (Fig. 2B, D). Likewise, the area of Sirius red staining rose from 0.25 to 0.50% ($P > 0.05$), 3.0% ($P < 0.05$), and 14.1% ($P < 0.0001$) in the early, middle, and late stages of infection, respectively (Fig. 2C, E). Serum ALT levels significantly increased at 120 dpi compared with uninfected group ($P < 0.01$). The serum levels of AST significantly increased at 40 dpi ($P < 0.01$), 80 dpi ($P < 0.01$) and 120 dpi ($P < 0.001$) compared with uninfected group (Table 1).

Profile of small RNAs in the livers of *E. multilocularis*-infected mice

A total of 20 samples were sequenced, among which the clean reads of each sample ranged from 17.15 to 25.08 M. The most abundant small RNAs in each group were miRNAs (42.3-54.92%), followed by non-annotated RNAs (37.28–42.77%), genes (5.16–14.45%), other small RNAs (0.91–3.18%) composed of Cis-reg, others, rRNA, snRNA, tRNA and other Rfam RNAs (Fig. 3).

Dynamic profile of miRNAs in the livers of *E. multilocularis*-infected mice in the early, middle, and late infection stages

A total of 61 (5.6%) stage-differentially expressed host-origin liver miRNAs were detected among the 1093 sequenced known miRNAs, including 29 up-regulated (47.5%) and 32 down-regulated miRNAs (52.5%) ($P < 0.05$, Supplementary Table 2). Small RNA-seq analysis identified 55 *Echinococcus*-derived miRNAs in the MirGeneDB database (Supplementary Table 3), with bioinformatic predictions indicating their potential involvement in modulating host-parasite crosstalk through mRNA targeting. However, further experimental validation is required to rule out sequencing-derived false positives. The heatmap and scatter diagram analysis revealed that abundant up-regulated miRNAs persisted in the early infection stage, while down-regulated miRNAs prevailed in the late infection stage (Fig. 4). The up-regulated miRNAs detected at the early, middle, and late infection stages accounted for 54.2% (13/24), 16.7% (4/24) and 8.3% (2/24) of the total, respectively. The mmu-miR-143-5p, mmu-miR-181b-2-3p, mmu-miR-301b-3p, and mmu-miR-1a-3p were co-expressed in both early and middle infection stages, while mmu-miR-16-1-3p was co-expressed in both early and late infection stages (Fig. 5A). The down-regulated miRNAs found at the early, middle, and late infection stages accounted for 7.4% (2/27), 11.1% (3/27), and 63% (17/27) of the total, respectively. The mmu-miR-1249-3p, mmu-miR-465a-3, mmu-miR-465b-3p, mmu-miR-465c-3p, and mmu-miR-465c-5p were co-expressed in both early and middle infection stages, while mmu-miR-1948-3p and mmu-miR-877-3p were co-expressed in both middle and late infection stages (Fig. 5B).

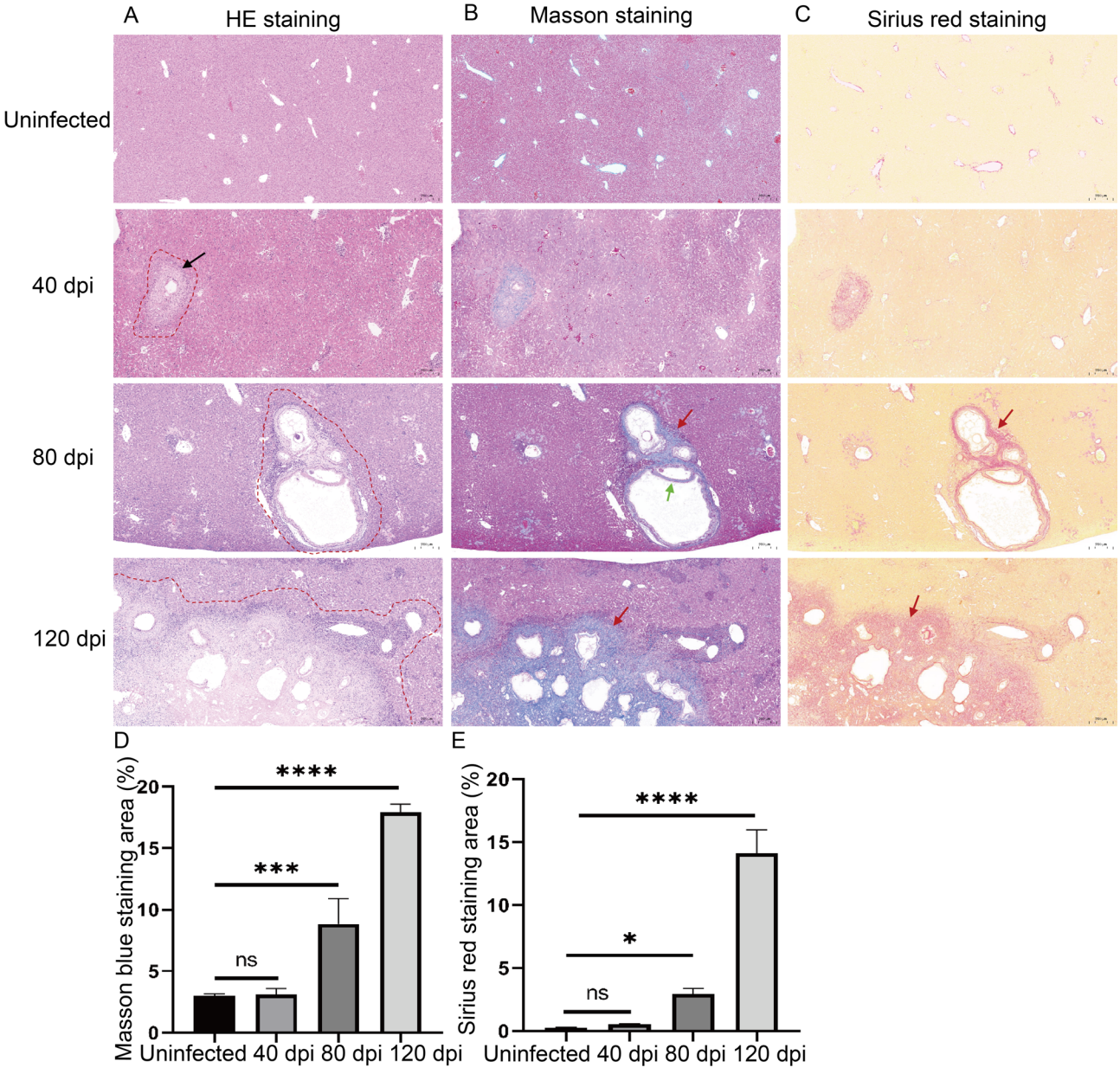

Fig. 2 Hepatic histopathological alterations in mice infected with *E. multilocularis* PSCs at different infection times. **A**: H&E staining of liver sections. **B**: Masson's trichrome staining of liver sections. **C**: Sirius staining of liver sections. **D**: Quantification of the fibrotic area of Masson trichrome staining. **E**: Quantification of the fibrotic area of Sirius Red staining. Note: Black arrow indicates inflammatory cells; Red dotted circle indicates the metocestodes; Red arrow indicates collagen deposits; Green arrow indicates germinal layer. NS: No statistical significance; *$P < 0.05$; *** $P < 0.001$; **** $P < 0.0001$

Functional enrichment of differentially expressed miRNA target genes

A total of 158 enriched terms were identified by GO analysis, including 109 biological process terms, 15 cellular component terms and 34 molecular function terms. In the early stage, the enriched gene function was predominantly associated with protein binding (GO:0005515), intracellular signal transduction (GO:0035556), and neuron projection (GO:0043005) (Fig. 6A). In the middle stage, enriched function was dominated by calmodulin binding (GO:0005516), ion channel binding (GO:0044325), and Z disc (GO:0030018) (Fig. 6B). In the late stage, the genes were primarily associated with protein binding (GO:0005515), plasma membrane (GO:0005886), and cell junction (GO:0030054) (Fig. 6C).

To explore the biological pathways of the differentially expressed miRNA target genes, we performed KEGG pathway enrichment analysis. In the early stage, genes were mainly enriched in Th17 cell differentiation, AMPK signaling pathway, calcium signaling pathway, etc. (Fig. 7A). In the middle stage, genes were mainly involved in proline signaling pathway, aldosterone synthesis

Table 1 Serum ALT and AST levels in the uninfected group and different infection stage groups

Index	Uninfected	40 dpi	80 dpi	120 dpi
ALT (U/L)	63.26 ± 6.11	74.73 ± 6.89	78.31 ± 9.56	91.44 ± 19.38**
AST (U/L)	66.91 ± 9.26	98.71 ± 13.31**	101.09 ± 19.6**	168.76 ± 8.82***

Note: Serum levels of ALT and AST were detected with commercial ALT and AST assay kits. The data are expressed as the means ± SD (n = 5) of three independent experiments.

*$P < 0.05$

**$P < 0.01$

***$P < 0.001$

secretion and Cushing's syndrome (Fig. 7B). In the late stage, genes were mainly involved in the regulation of ECM-receptor interactions, TGF-β signaling pathway and human papillomavirus infection (Fig. 7C). There were very few up-regulated miRNAs in the middle infection stage, thus no functional enrichment analysis results were obtained.

Predicted miRNA-target gene-pathway networks

To further understand the regulation of the stage-differentially expressed miRNAs and their putative target gene-associated pathways, the interaction network was performed using Cytoscape v3.8.2 software. In the network at early infection stage, a total of 15 miRNAs, 122 putatively targeting genes and 20 pathways were enriched (Supplementary Fig. 1), in which the top enriched miRNA and predicted target gene were mmu-miR-1247-5p (score = 30) and Proto-oncogene tyrosine-protein kinase SRC (*Src*, score = 17), respectively (Fig. 8A, and Supplementary Table 4), being predominantly associated with the Rab 1 signaling pathway (Supplementary Table 5). In network at middle infection stage, a total of 7 miRNAs, 55 putatively targeting genes and 20 pathways were enriched (Supplementary Fig. 2), among them, the top miRNA and targeting gene were mmu-miR-149-5p (score = 37) and Jagged canonical notch ligand 1 (*Jag 1*, score = 3), respectively (Fig. 8B and Supplementary Table 6) and which were predominantly associated with the Notch signaling pathway (Supplementary Table 7). In

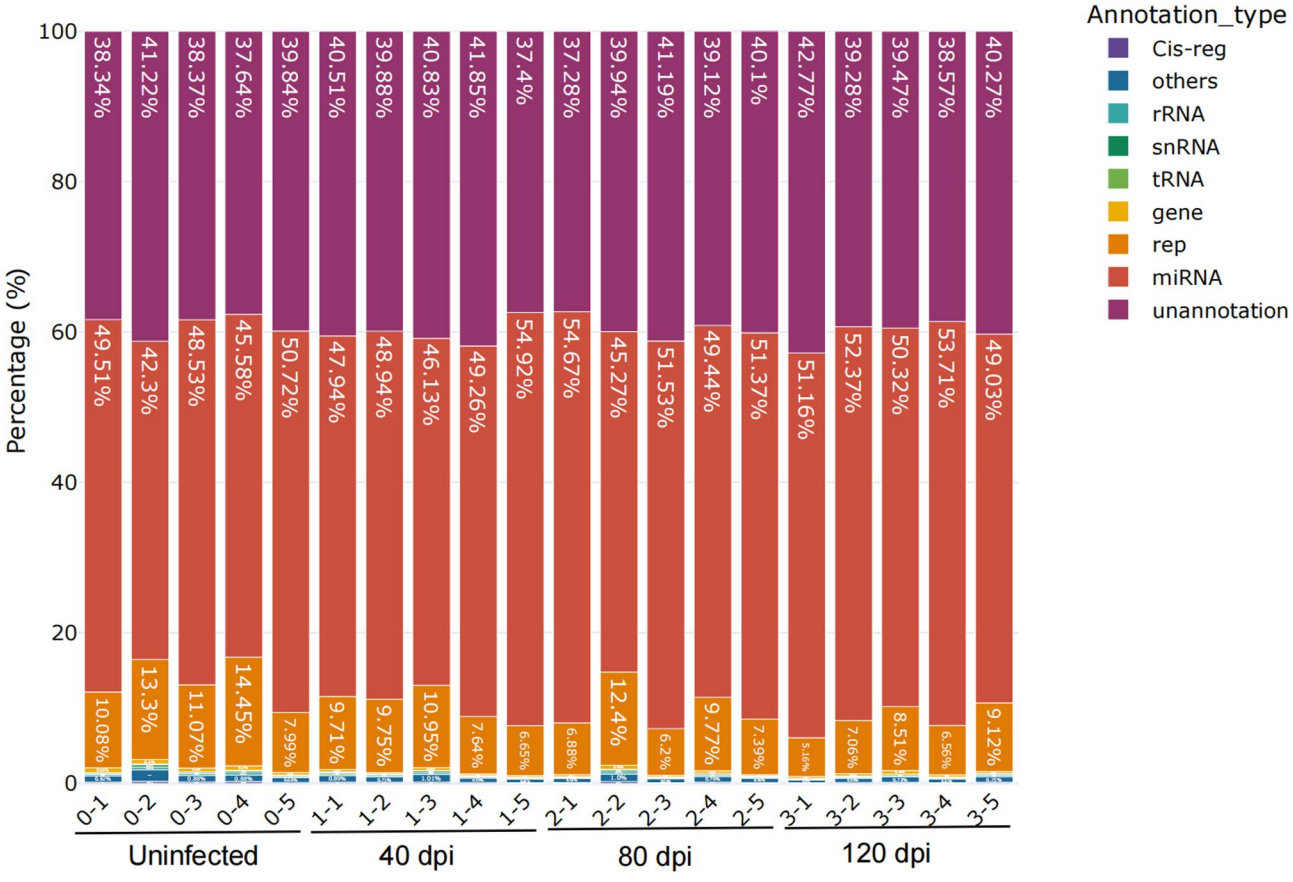

Fig. 3 Profile of small RNA proportions in the livers of *E. multilocularis*-infected mice. Note: The percentages of miRNA, Cis-reg, rRNA, tRNA, snRNA, rep, gene, others and unannotation sequences identified by small RNA sequencing in the three stages of infection (40, 80 and 120 dpi, 5 mice in each group). 0: Uninfected; 1: 40 dpi; 2: 80 dpi; 3: 120 dpi. Cis-reg: cis-regulatory elements; rRNA: ribosomal RNA; tRNA: transfer RNA; snRNA: small nuclear RNA; rep: repeat regions

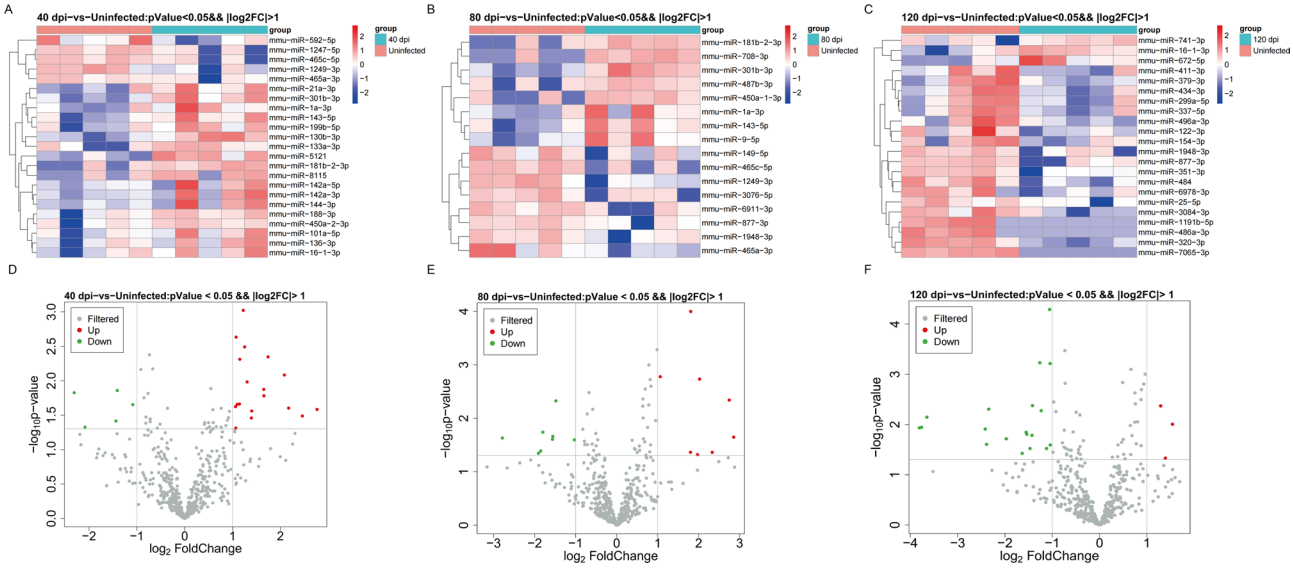

Fig. 4 Heatmap and scatter diagram of differentially expressed miRNAs in each group. **A**: Heatmap of miRNA expression profiling in 40 dpi VS uninfected; **B**: Heatmap of miRNA expression profiling in 80 dpi VS uninfected; **C**: Heatmap of miRNA expression profiling in 120 dpi VS uninfected; **D**: Scatter diagram of miRNA expression profiling in 40 dpi VS uninfected; **E**: Scatter diagram of miRNA expression profiling in 80 dpi VS uninfected; **F**: Scatter diagram of miRNA expression profiling in 120 dpi VS uninfected

the late infection stage network, a total of 19 miRNAs, 101 putatively targeting genes and 20 pathways were enriched (Supplementary Fig. 3), with a top interaction of mmu-miR-299a-5p (score = 14)-mitogen-activated protein kinase 1 (*Mapk1*, score = 35)-human papillomavirus infection pathway (score = 14) (Fig. 8C and Supplementary Table 8). In addition, the network of the whole infection period showed a total of 6 miRNAs, 23 target genes and 20 pathways enrichment (Supplementary Fig. 4), among them, the hub network was mmu-miR-122-3p (score = 18)-Serum response factor (*Srf*, score = 1)-MAPK pathway (score = 1) hub network. (Fig. 8D, and Supplementary Table 9).

STEM analysis and quantitative real-time PCR validation of miRNAs

A set of 50 microRNA-seq data profiles (ID0 to 49) emerged from STEM analysis. Among these, 7 profiles (ID26, 11, 9, 34, 41, 38, 44) displayed significant changes ($P < 0.05$) (Supplementary Fig. 5). Profiles ID 26, 9, and 34 exhibited a gradual decrease over infection time, while profiles ID41 and 44 showed a gradual increase. However, profile ID41 peaked at 80 days post-infection, whereas profile ID44 peaked at 40 dpi. Profile ID38 microRNA-seq did not reveal any significantly differentially expressed miRNAs compared to the uninfected group; hence, qRT-PCR verification was not pursued for this profile. The expression levels of mmu-miR-299a-5p, mmu-miR-6978-3p, mmu-miR-122-3p, mmu-miR-154-3p, mmu-miR-1a-3p, and mmu-miR-142a-5p in these 6 significant profiles were successfully validated by qRT-PCR. It is noteworthy that the expression level of mmu-miR-6978-3p in profile ID11 was too low for confirmation via qRT-PCR analysis (Fig. 9A, B).

Discussion

In this study, we examined the temporal dynamics of hepatic miRNAs in mice infected with *E. multilocularis* at early (40 dpi), middle (80 dpi), and late (120 dpi) stages. The aim of this study was to identify the specific miRNA profiles associated with different stages of AE progression. We successfully established an *E. multilocularis*-infected mouse model via in situ surgical intrahepatic implantation and collected liver samples at three time points of infection. Pathology of the mouse liver revealed increased inflammatory cell infiltration in the early stage of infection, and fibrous bridges or granuloma nodules were observed in the middle infection stage, while the texture of the liver appeared to harden in the late infection stage. Moreover, the serum ALT and AST levels gradually elevated with prolonged infection *E. multilocularis*; above all, both pathological and physiological changes worsened with increasing duration of infection. Thus, a progressive increase in fibrosis could be seen as the infection progressing.

To uncover the molecular mechanisms underlying prolonged host infection, we analyzed the dynamic changes in miRNA profiles over the infection period. Among 68 differentially expressed miRNAs, STEM analysis identified 50 profiles, with 7 showing significant changes during the infection period. It was found that up-regulated miRNAs were abundant in the early stage of infection,

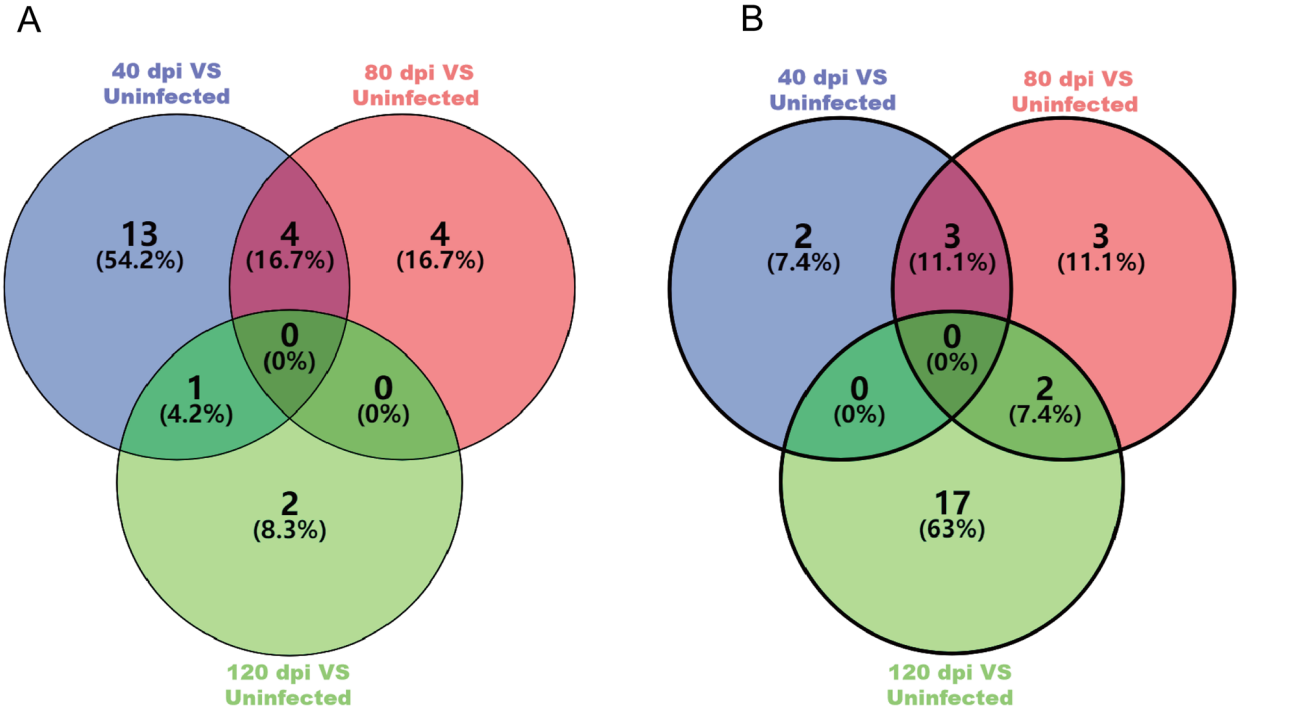

Group comparison	Up-regulated miRNAs	Down-regulated miRNAs
40 dpi VS Uninfected	mmu-miR-101a-5p; mmu-miR-130b-3p; mmu-miR-133a-3p; mmu-miR-136-3p; mmu-miR-142a-3p; mmu-miR-142a-5p; mmu-miR-143-5p*; mmu-miR-144-3p; mmu-miR-16-1-3p $; mmu-miR-181b-2-3p*; mmu-miR-188-3p; mmu-miR-199b-5p; mmu-miR-1a-3p*; mmu-miR-21a-3p; mmu-miR-301b-3p*; mmu-miR-450a-2-3p; mmu-miR-5121; mmu-miR-8115.	mmu-miR-1247-5p; mmu-miR-1249-3p*; mmu-miR-465a-3p>mmu-miR-465b-3p>mmu-miR-465c-3p*; mmu-miR-465c-5p*; mmu-miR-592-5p.
80 dpi VS Uninfected	mmu-miR-143-5p*; mmu-miR-181b-2-3p*; mmu-miR-1a-3p*; mmu-miR-301b-3p*; mmu-miR-450a-1-3p; mmu-miR-487b-3p; mmu-miR-708-3p; mmu-miR-9-5p.	mmu-miR-1249-3p*; mmu-miR-149-5p; mmu-miR-1948-3p#; mmu-miR-3076-5p; mmu-miR-465a-3p>mmu-miR-465b-3p>mmu-miR-465c-3p*; mmu-miR-465c-5p*; mmu-miR-6911-3p; mmu-miR-877-3p#.
120 dpi VS Uninfected	mmu-miR-16-1-3p$; mmu-miR-672-5p; mmu-miR-741-3p.	mmu-miR-1191b-5p; mmu-miR-122-3p; mmu-miR-154-3p; mmu-miR-1948-3p#; mmu-miR-25-5p; mmu-miR-299a-5p; mmu-miR-3084-3p; mmu-miR-320-3p; mmu-miR-337-5p; mmu-miR-351-3p; mmu-miR-379-3p; mmu-miR-411-3p; mmu-miR-434-3p; mmu-miR-484; mmu-miR-486a-3p; mmu-miR-496a-3p; mmu-miR-6978-3p; mmu-miR-7065-3p; mmu-miR-877-3p#.
Note: *: Both shared in 40 dpi and 80 dpi; $: Both shared in 40 dpi and 120 dpi. #: Both shared in 80 dpi and 120 dpi.		

Fig. 5 Venn diagram of differentially expressed miRNAs in each infection stage. **A**: Venn diagram of the up-regulated miRNAs in each group; **B**: Venn diagram of the down-regulated miRNAs in each group

whereas down-regulated miRNAs predominated in the late stage of infection. These findings were consistent with Jin et al.'s finding, showing 93.5% (43/46) down-regulation in *E. multilocularis*-infected mouse liver at 90 days post-infection [18]. The study revealed that differentially expressed miRNAs and their target genes were mainly associated with Th17 cell differentiation and the AMPK signaling pathway during the early infection stage. This association may be related to immune regulation during *E. multilocularis* infection. At the onset of infection, the host generates a strong immune response against foreign pathogens, while the parasite recruits myeloid cells, such as monocytes and dendritic cells, to trigger a pro-inflammatory Th1/Th17 response aimed at controlling parasite growth or eliminating lesions [37]. These findings indicate a predominance of immunoregulation-related miRNAs and pathways, including intracellular signal transduction and Th17 cell differentiation, in the initial phases of infection, consistent with Lin et al.'s findings [14]. In the middle infection stage, target genes were predominantly involved in pathways related to host metabolism, particularly hormone-related pathways, suggesting that host liver metabolism is reprogrammed after *E. multilocularis* infection, favoring parasite growth [10]. During the late infection stage, the growth of *E. multilocularis* larvae leads to the formation of protective

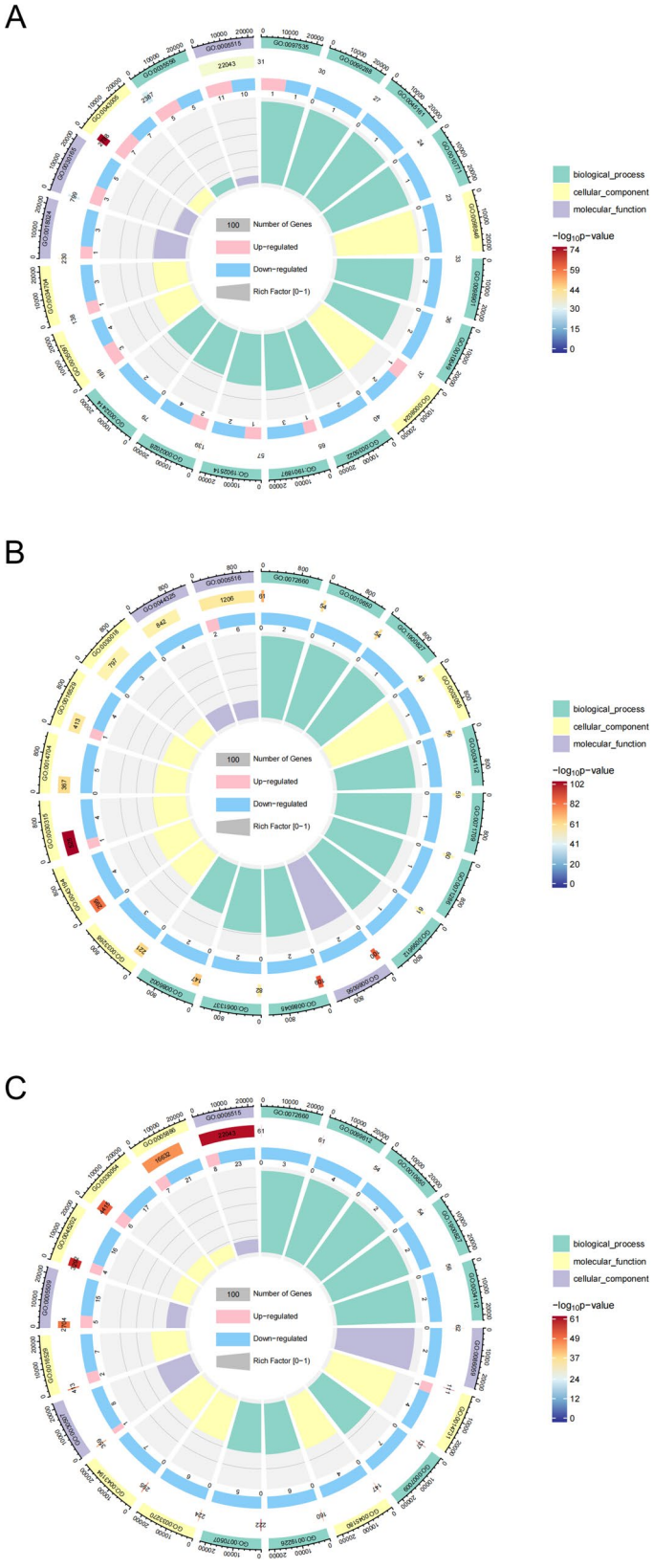

Fig. 6 (See legend on next page.)

(See figure on previous page.)

Fig. 6 GO enrichment of differentially expressed genes. **A**: GO annotation of 40 dpi; **B**: GO annotation of 80 dpi; **C**: GO annotation of 120 dpi. Note: First ring: Displays the top 20 significantly enriched GO terms (ID labels). Second ring: Represents the total count of differentially expressed genes (DEGs) assigned to each GO term. Third ring: Visualizes the proportion of up-regulated (light red) and down-regulated (light blue) genes within each term. Fourth ring: Corresponds to the RichFactor value (calculated as DEGs per term/total annotated genes per term). Background gridlines (spaced at 0.2 intervals) provide reference for RichFactor magnitude interpretation

layers, namely, Laminal layer and Germinal layer, which resist the host's immune response and facilitate parasite survival and metacestode growth [38]. A transition to a mixed Th1/Th2 phenotype occurs during this stage, enabling the parasite's survival and metacestode growth [37]. Therefore, many miRNAs were down-regulated and target gene and pathways were enriched mainly in ECM-receptor interactions, TGF-β signaling pathway and human papillomavirus infection. Numerous prior investigations have demonstrated that the development of liver fibrosis in AE is strongly influenced by the participation of TGF-β [2, 13, 16], which suggests that most of the pathways enriched in the late infection stage are related to the regulation of liver fibrosis. This finding was consistent with the pathological findings of host liver fibrosis at the late infection stage of *E. multilocularis*.

The putative hub miRNA-target gene-pathway networks identified in the present study provides clues to further understand the infection and pathogenesis of AE. Networks mmu-miR-1247-5p-*Src*-Rap1 signaling pathway, mmu-miR-149-5p-*Jag1*-Notch signaling pathway, mmu-miR-299a-5p-*Mapk*-Human papillomavirus infection pathway were predicted to be associated with disease progression, while the mmu-miR-122-3p-*Srf*-MAPK signaling pathway exhibited dynamic changes throughout the entire infection stage. Proto-oncogene tyrosine kinase SRC (*Src*), a risk gene, predicted to be targeted by mmu-miR-1247-5p detected in this study in the early infection stage was previously reported to play a crucial role in the parasitic infection. SRC kinase inhibitors were reported as an alternative drug strategy for the treatment of schistosomiasis [39]. Moreover, SRC kinases were identified as potential serological diagnostic markers of active cystic echinococcosis [40]. However, the regualtion of mmu-miR-1247-5p to *Src* gene in AE requires further experimental verification. At the middle infection stage, *Jag1* is a putative hub gene that is likely targeted by mmu-miR-149-5p and regulating the Notch signaling pathway. Studies indicate that miR-149-5p protects rats from injury by regulating Notch2 signaling pathways involved in inflammation and apoptosis [41]. Additionally, *Jag1* has been suggested to be associated with the liver granuloma and fibrosis in schistosomiasis by regulating the Notch signaling pathway [42], Therefore, we speculate whether mmu-miR-149-5p-*Jag1*-Notch signaling pathway has an important regulatory role in AE warrants further investigation. In the late infection stage, it was found that *Mapk1* emerges as a predicted hub target gene primarily targeted by mmu-miR-299a-5p and regulated in human papillomavirus infection pathway. Previous research demonstrated that the ERK1/2 (also termed MAPK3/1)-AKT axis functions as a critical switch in regulating profibrotic phenotypes in chronic liver injury mice [43]. Consequently, we hypothesize that mmu-miR-299a-5p leads to liver fibrosis in AE by targeting the *Mapk1* gene, which needs further experimental verification. Throughout the whole infection stage, the expression level of mmu-miR-122-3p progressively declined over time, whereas the expression level of the predicted target gene *Srf* correspondingly increased. This up-regulation of *Srf* may thereby modulated the MAPK pathway. Previous studies have shown that *E. multilocularis*-derived signals efficiently activate MAPK signaling pathways in host liver cells, suggesting that MAPK signaling pathway plays a central role in *E. multilocularis* infection [44]. It has been established that miR-122-5p is significantly down-regulated in fibrotic livers, while, its two common target genes, type I TGF-β receptor(*TGFβR1*) and *TGFβR2*, are up-regulated. This up-regulation activates the TGF-β signaling pathway, ultimately leads to the progress of liver fibrosis [45]. The research showed TGF-β/Smad signaling pathway was activated during the chronic infection of *E. multilocularis* [16] and also regarded as the drug target of AE [46]. Therefore, we hypothesize that the sustained down-regulation of miR-122-3p over the course of infection time in this study may be associated with the progressive aggravation of liver fibrosis in AE. However, the precise underlying mechanisms need further investigation. Serum response factor (*Srf*) is a pivotal mediator of fibroblast transcription, increasing evidence suggests that *Srf* plays a critical role in the pathogenesis of liver fibrosis, and it has been documented that miR-122 can regulate the expression of the *Srf* gene to inhibit the development of liver fibrosis [47–49]. Referring to the above results, we speculate that the miR-122-3p may influence the liver fibrosis in *E. multilocularis* infected mouse by targeting to *Srf* hub gene and regulating MAPK signaling pathway. It could be a potential diagnostic marker and therapeutic target for AE if this dysregulation is also detectable in circulation, but further research is needed. This study highlights significant findings regarding the regulation of *Src*, *Jag1*, *Mapk1* and *Srf* genes, along with their associated miRNAs and pathways in different infection stages of *E. multilocularis*. These insights suggest that core miRNAs and putative target genes could serve as effective targets

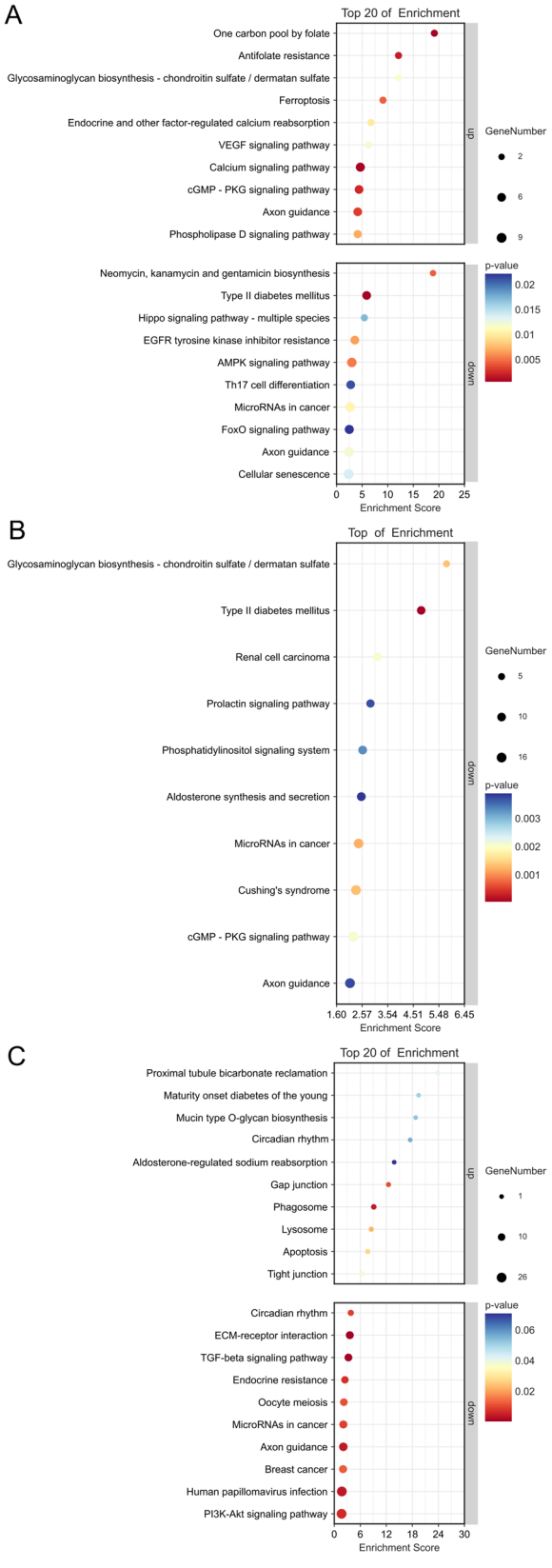

Fig. 7 KEGG enrichment of differentially expressed genes. **A**: KEGG enrichment of differentially expressed genes in 40 dpi; **B**: KEGG enrichment of differentially expressed genes in 80 dpi; **C**: KEGG enrichment of differentially expressed genes in 120 dpi. Note: up: top 10 enrichment pathways of upregulated miRNA target genes; down: top 10 enrichment pathways of down-regulated miRNA target genes

for vaccine and drug development to tackle AE and other parasite infections.

The current study demonstrated that miRNAs exhibit dynamic expression profiles throughout the entire infection time, displaying time-specific patterns during the early, middle, and late stages of infection. Consequently, these altered miRNAs, target genes, and pathways may provide potential targets for future development of diagnostics, vaccines, and drugs. The above mentioned information presents numerous potential indications regarding the extent of complex molecular alterations in the host liver during long-term infection with *E. multilocularis*. Our study has several limitations related to the use of search strategies. First, the expression of only a few genes has been verified, and the expression of other genes, especially those with low expression levels, needs to be verified with more sensitive methods. Second, we identified a changing profile of miRNAs that expressed during infection, and found the core regulated target genes and pathways, but the specific functions of these miRNAs need to be further verified. Additionally, to address the effect of inter-individual and tissue heterogeneity in murine hepatic samples, five biological replicates per experimental groups were incorporated. Liver tissues from each mouse were systematically collected from three distinct regions (lobes), and pooled to generate representative composite samples for sequencing, thereby mitigating sampling bias and regional expression variability.

Conclusion

A total of 61 liver miRNAs originating from the host exhibited differential expression compared to uninfected liver tissue, comprising 29 significantly up-regulated and 32 significantly down-regulated miRNAs. The results obtained from bioinformatics prediction were consistent with the pathological findings at each infection stage. During the early stage, there was a predominant enrichment of immune response pathways, while the middle infection stage exhibited enrichment in metabolism, particularly hormone-related pathways. In the late infection stage, pathways related to liver fibrosis were enriched. The temporal dynamic changes of miRNAs in mouse liver and their target genes' interaction in KEGG pathway network responding to

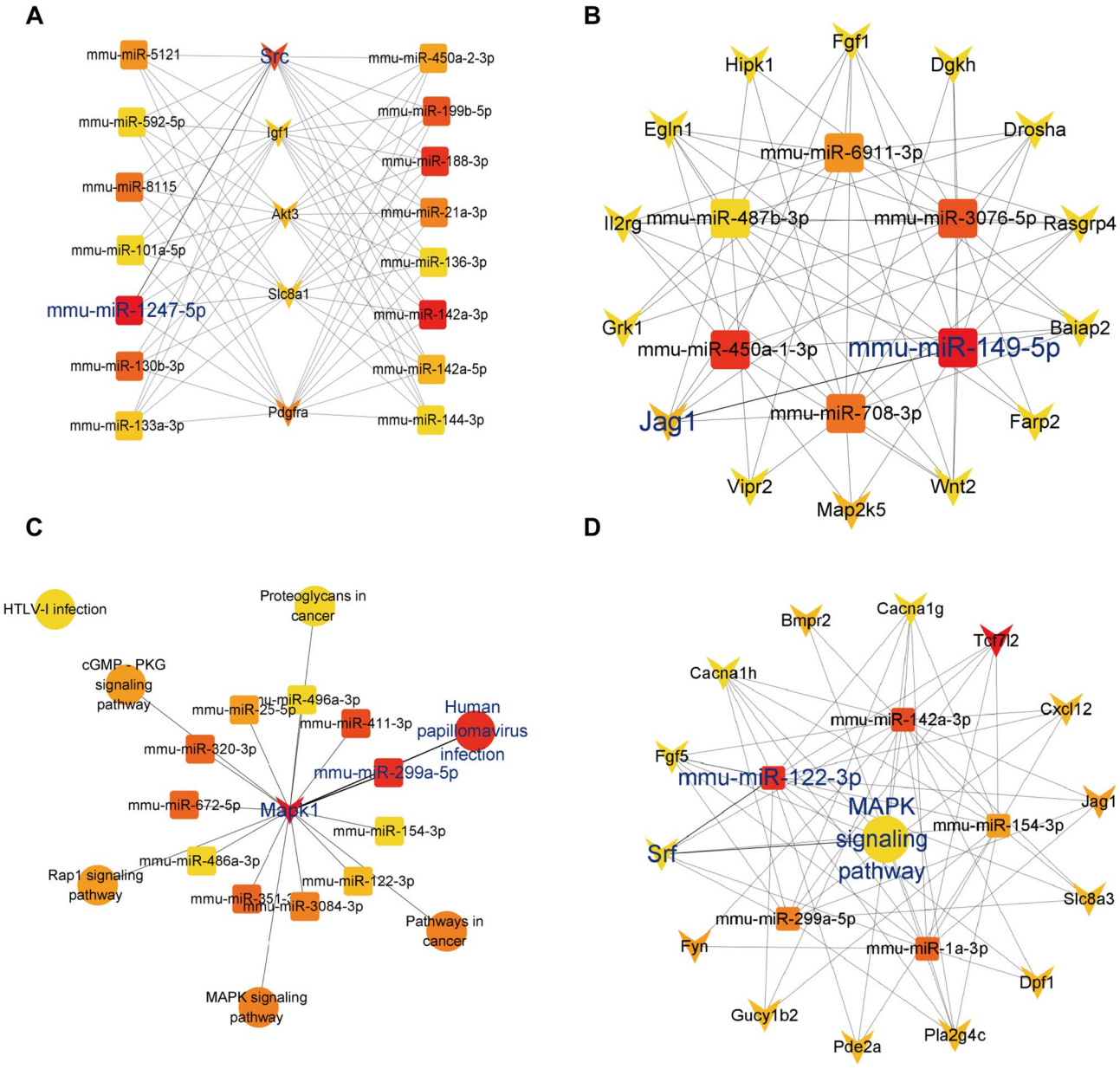

Fig. 8 Predicted miRNA-target gene-pathway networks. A: Subnetwork of 40 dpi; B: Subnetwork of 80 dpi; C: Subnetwork of 120 dpi; D: Subnetwork of all infection stages. In the network visualization, the squares represent miRNAs, the circles represent KEGG pathways, and the triangles represent target genes. Hub miRNAs and their target gene-pathway interactions were represented by blue bold edges. Node centrality scores were color-coded according to a gradient from red (highest), transitioning through orange and yellow, to blue (lowest) Note: The score of the KEGG pathways enriched in the early and middle stages of infection was relatively low, so they were not enriched in the subnetwork screened by BottleNeck. According to the KEGG pathway analysis results, the *Src* and *Jag1* genes were mainly involved in the Rab1 and Notch signaling pathways

different infection stages of *E. multilocularis* may be conducive to understanding the pathogenic mechanism of the parasite. We identified at least four significant putative miRNA-target gene-pathway networks, involving mmu-miR-1247-5p-*Src*-Rap1 signaling pathway, mmu-miR-149-5p-*Jag1*-Notch signaling pathway, mmu-miR-149-5p-*Mapk1*-Human papillomavirus infection pathway, and mmu-miR-122-3p-*Srf*-MAPK signaling pathway. The first three signaling hubs were found to be associated with disease progression, while the last interaction exhibited dynamic changes throughout the entire infection stage. These findings provide a foundation for potential advancements in vaccine and drug development.

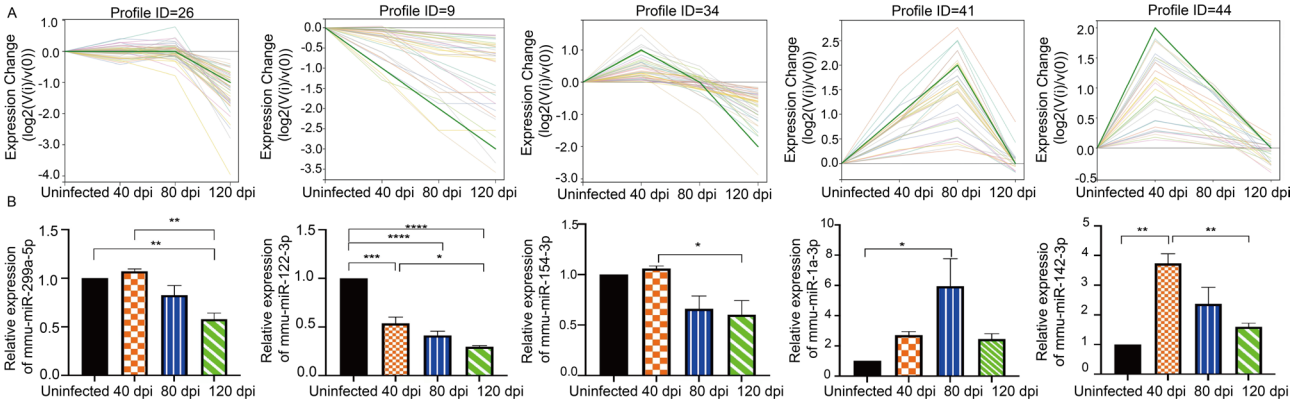

Fig. 9 QRT–PCR validation of miRNA expression. **A**: STEM analysis of the miRNAs: Significant expression trend chart. The vertical axis represents the expression difference relative to the first time point (uninfected), and the horizontal axis represents the different time points, where the thick green line represents the expression trend. **B**: qRT–PCR validation of miRNAs. Note: **P* < 0.05, ***P* < 0.01, ****P* < 0.001, *****P* < 0.0001

Abbreviations

AE	Alveolar echinococcosis
E. multilocularis	*Echinococcus multilocularis*
WHO	World Health Organization
STEM	Short Time-series Expression Miner
NGS	Next-generation sequencing
qRT-PCR	Quantitative real-time PCR
DEGs	Differentially expressed mRNAs
Src	Proto-oncogene tyrosine kinase SRC
Jag 1	Jagged canonicalncotch ligand 1
MAPK signaling pathway	Mitogen-activated protein kinase signaling pathway
Mapk1	Mitogen-activated protein kinase 1
Srf	Serum response factor

Supplementary Information

The online version contains supplementary material available at https://doi.org/10.1186/s12864-025-12049-z.

Supplementary Material 1.

Supplementary Material 2.

Acknowledgements

Not applicable.

Authors' contributions

TZ and WH designed the study. HG, YC, CL, XM, GZ and JX carried out the experiments. YC, TZ and JG analyzed data. WH and TZ provided experimental material. YC, TZ, ZF and BB wrote the manuscript. TZ and YC revised the manuscript. All authors contributed to the article and approved the submitted version.

Funding

This work was supported by the National Key Research and Development Program of China (No. 2021YFC2300800, 2021YFC2300803) to TZ, State Key Laboratory for Reproductive Regulation and Breeding of Grassland Livestock (No. 2021KF0301) to TZ, and NHC Key Laboratory of Echinococcosis Prevention and Control (No. 2024WZK1002) to TZ. The funders had no role in the study design, data collection, data analysis, data interpretation, or the writing of this report.

Data availability

The original contributions presented in the study are included in the article/supplementary material. The raw data has been submitted to the National Center for Biotechnology Information (NCBI) Sequence Read Archive (SRA) under Submission ID: SRP547172 and BioProject accession number PRJNA1186565. The data can be accessed through the following link: https://www.ncbi.nlm.nih.gov/sra/PRJNA1186565.

Declarations

Ethics approval and consent to participate

SPF KM mice (8 weeks, female, weight 20 ± 2 g) were purchased from Shanghai Jiesijie Experimental Animal Co., LTD. (production license Certificate No: SCXK (Shanghai) 2018-0004). These mice were bred under specified pathogen-free conditions. The keeping of mice and the experimental protocol of this study were approved by the Animal Ethics Committee of Parasitic Diseases Prevention and Control Center of China (Authorization Number: IPD-2021-27) and the Institutional Animal Care and Use Committee at the Inner Mongolia University (No. SCXK (Mongolia) 2020-0006). All efforts were made to minimize suffering of mice.

Consent for publication

Not applicable.

Competing interests

The authors declare no competing interests.

Author details

[1]The State Key Laboratory of Reproductive Regulation and Breeding of Grassland Livestock, School of Life Sciences, Inner Mongolia University, Hohhot 010010, China
[2]National Institute of Parasitic Diseases, Chinese Center for Disease Control and Prevention (Chinese Center for Tropical Diseases Research); National Key Laboratory of Intelligent Tracking and Forecasting for Infectious Diseases; National Health Commission Key Laboratory of Parasite and Vector Biology; WHO Collaborating Center for Tropical Diseases; National Center for International Research on Tropical Diseases, Ministry of Science and Technology, Shanghai 200025, China
[3]National Health Commission Key Laboratory of Echinococcosis Prevention and Control, Tibet Autonomous Region Center for Disease Control and Prevention, Lhasa, Tibet Autonomous Region, China
[4]State Key Laboratory of Genetic Engineering, Ministry of Education Key Laboratory of Contemporary Anthropology, Collaborative Innovation Center for Genetics and Development, School of Life Sciences, Fudan University, Shanghai 200025, China

[5]School of Global Health, Chinese Center for Tropical Diseases Research, Shanghai Jiao Tong University School of Medicine, Shanghai 200025, China

Received: 28 October 2024 / Accepted: 25 August 2025
Published online: 21 October 2025

References

1. Eckert J, Deplazes P. Biological, epidemiological, and clinical aspects of echinococcosis, a zoonosis of increasing concern. Clin Microbiol Rev. 2004;17(1):107–35.
2. Yang N, Ma W, Ke Y, Liu H, Chu J, Sun L, et al. Transplantation of adipose-derived stem cells ameliorates *Echinococcus multilocularis*-induced liver fibrosis in mice. PLoS Negl Trop Dis. 2022;16(1):e0010175.
3. Deplazes P, Rinaldi L, Alvarez Rojas CA, Torgerson PR, Harandi MF, Romig T, Antolova D, Schurer JM, Lahmar S, Cringoli G, et al. Global distribution of alveolar and cystic echinococcosis. Adv Parasitol. 2017;95:315–493.
4. Knapp J, Lallemand S, Monnien F, Felix S, Valmary-Degano S, Courquet S, Demonmerot F, Heyd B, Turco C, Doussot A, et al. Molecular diagnosis of alveolar echinococcosis in patients based on frozen and formalin-fixed paraffin-embedded tissue samples. Parasite. 2022;29:4.
5. Liu C, Fan H, Ma J, Ma L, Ge RL. In vitro and in vivo efficacy of thiacloprid against *Echinococcus multilocularis*. Parasit Vectors. 2021;14(1):450.
6. Gloor S, Candinas D, Beldi G, Lachenmayer A. Laparoscopic resection of hepatic alveolar echinococcosis: a single-center experience. PLoS Negl Trop Dis. 2022;16(9):e0010708.
7. Stefaniak M, Derda M, Zmora P, Nowak SP. Risk factors and the character of clinical course of the *Echinococcus multilocularis* infection in patients in Poland. Pathogens. 2023. https://doi.org/10.3390/pathogens12020199.
8. Protzer U, Maini MK, Knolle PA. Living in the liver: hepatic infections. Nat Rev Immunol. 2012;12(3):201–13.
9. Vuitton DA, Gottstein B. *Echinococcus multilocularis* and its intermediate host: a model of parasite-host interplay. J Biomed Biotechnol. 2010. https://doi.org/10.1155/2010/923193.
10. Zhang C, Wang J, Lu G, Li J, Lu X, Mantion G, et al. Hepatocyte proliferation/growth arrest balance in the liver of mice during *E. multilocularis* infection: a coordinated 3-stage course. PLoS One. 2012;7(1):e30127.
11. Gao HJ, Pang HS, Sun XD, Zhang T, Jing T, Wang XL, et al. Effects of persistent *Echinococcus multilocularis* infections on hepatic fibrosis in mice. Zhongguo Xue Xi Chong Bing Fang Zhi Za Zhi. 2021;33(1):54–61.
12. Vuitton DA. The ambiguous role of immunity in echinococcosis: protection of the host or of the parasite? Acta Trop. 2003;85(2):119–32.
13. Wen H, Vuitton L, Tuxun T, Li J, Vuitton DA, Zhang W, et al. Echinococcosis: advances in the 21st century. Clin Microbiol Rev. 2019. https://doi.org/10.1128/CMR.00075-18.
14. Lin R, Lu G, Wang J, Zhang C, Xie W, Lu X, et al. Time course of gene expression profiling in the liver of experimental mice infected with *Echinococcus multilocularis*. PLoS One. 2011;6(1):e14557.
15. Nian X, Li L, Ma X, Li X, Li W, Zhang N, et al. Understanding pathogen-host interplay by expression profiles of LncRNA and mRNA in the liver of *Echinococcus multilocularis*-infected mice. PLoS Negl Trop Dis. 2022;16(5):e0010435.
16. Pang N, Zhang F, Ma X, Zhu Y, Zhao H, Xin Y, et al. TGF-beta/Smad signaling pathway regulates Th17/Treg balance during *Echinococcus multilocularis* infection. Int Immunopharmacol. 2014;20(1):248–57.
17. Britton C, Winter AD, Marks ND, Gu H, McNeilly TN, Gillan V, Devaney E. Application of small RNA technology for improved control of parasitic helminths. Vet Parasitol. 2015;212(1–2):47–53.
18. Jin X, Guo X, Zhu D, Ayaz M, Zheng Y. Mirna profiling in the mice in response to *Echinococcus multilocularis* infection. Acta Trop. 2017;166:39–44.
19. Cai P, Gobert GN, McManus DP. Micrornas in parasitic helminthiases: current status and future perspectives. Trends Parasitol. 2016;32(1):71–86.
20. Guo X, Zheng Y. Profiling of miRNAs in mouse peritoneal macrophages responding to *Echinococcus multilocularis* infection. Front Cell Infect Microbiol. 2020;10:132.
21. Boubaker G, Strempel S, Hemphill A, Muller N, Wang J, Gottstein B, et al. Regulation of hepatic microRNAs in response to early stage *Echinococcus multilocularis* egg infection in C57BL/6 mice. PLoS Negl Trop Dis. 2020;14(5):e0007640.
22. Liu T, Wang L, Li H, Li Y, Chen G, Pu G, et al. CircRNA expression pattern and circRNA-miRNA-mRNA network in hcs, hscs, and KCs of murine liver after *Echinococcus multilocularis* infection. Front Vet Sci. 2022;9:825307.
23. Gao HJ, Sun XD, Luo YP, Pang HS, Ma XM, Zhang T, et al. Anti-echinococcal effect of verapamil involving the regulation of the calcium/calmodulin-dependent protein kinase II response *in vitro* and in a murine infection model. Parasit Vectors. 2021;14(1):108.https://doi.org/10.1186/s13071-021-04618-4
24. Wang T, Li W, Zhang Y, Xu X, Qiang L, Miao W, et al. Bioprinted constructs that simulate nerve-bone crosstalk to improve microenvironment for bone repair. Bioact Mater. 2023;27:377–93.
25. Wei C, Sun Y, Zeng F, Chen X, Ma L, Liu X, et al. Exosomal miR-181d-5p derived from Rapamycin-conditioned MDSC alleviated allograft rejection by targeting KLF6. Adv Sci (Weinh). 2023;10(34):e2304922.
26. Griffiths-Jones S, Bateman A, Marshall M, Khanna A, Eddy SR. Rfam: an RNA family database. Nucleic Acids Res. 2003;31(1):439–41.
27. Chen N. Using repeatmasker to identify repetitive elements in genomic sequences. Curr Protoc Bioinf. 2004, Chap. 4:Unit 4 10.
28. Kozomara A, Griffiths-Jones S. MiRBase: annotating high confidence MicroRNAs using deep sequencing data. Nucleic Acids Res. 2014;42(Database issue):D68-73.
29. Friedlander MR, Mackowiak SD, Li N, Chen W, Rajewsky N. Mirdeep2 accurately identifies known and hundreds of novel microRNA genes in seven animal clades. Nucleic Acids Res. 2012;40(1):37–52.
30. Herrera MC, Tognetti S, Riera A, Zech J, Clarke P, Fernandez-Cid A, et al. A reconstituted system reveals how activating and inhibitory interactions control DDK dependent assembly of the eukaryotic replicative helicase. Nucleic Acids Res. 2015;43(21):10238–50.
31. Langmead B. Aligning short sequencing reads with bowtie. Curr Protoc Bioinf 2010 Chap 11:Unit 11 17.
32. Love MI, Huber W, Anders S. Moderated estimation of fold change and dispersion for RNA-seq data with DESeq2. Genome Biol. 2014;15(12):550.
33. Abel Y, Rederstorff M. Stem-loop qRT-PCR-based quantification of miRNAs. Methods Mol Biol. 2021;2300:59–64.
34. Schefe JH, Lehmann KE, Buschmann IR, Unger T, Funke-Kaiser H. Quantitative real-time RT-PCR data analysis: current concepts and the novel gene expression's CT difference formula. J Mol Med (Berl). 2006;84(11):901–10.
35. Shannon P, Markiel A, Ozier O, Baliga NS, Wang JT, Ramage D, Amin N, Schwikowski B, Ideker T. Cytoscape: a software environment for integrated models of biomolecular interaction networks. Genome Res. 2003;13(11):2498–504.
36. Yu H, Kim PM, Sprecher E, Trifonov V, Gerstein M. The importance of bottlenecks in protein networks: correlation with gene essentiality and expression dynamics. PLoS Comput Biol. 2007;3(4):e59.
37. Wang J, Goepfert C, Mueller N, Piersigilli A, Lin R, Wen H, et al. Larval *Echinococcus multilocularis* infection reduces dextran sulphate sodium-induced colitis in mice by attenuating T helper type 1/type 17-mediated immune reactions. Immunology. 2018;154(1):76–88.
38. Ingold K, Gottstein B, Hemphill A. Identification of a laminated layer-associated protein in *Echinococcus multilocularis* metacestodes. Parasitology. 1998;116(Pt 4):363–72.
39. Chienwichai P, Ampawong S, Adisakwattana P, Thiangtrongjit T, Limpanont Y, Chusongsang P, et al. Effect of praziquantel on *schistosoma mekongi* proteome and phosphoproteome. Pathogens. 2020. https://doi.org/10.3390/pathogens9060417.
40. Fratini F, Tamarozzi F, Macchia G, Bertuccini L, Mariconti M, Birago C, et al. Proteomic analysis of plasma exosomes from cystic echinococcosis patients provides in vivo support for distinct immune response profiles in active vs inactive infection and suggests potential biomarkers. PLoS Negl Trop Dis. 2020;14(10):e0008586.
41. Wang X, Xu Q, Wang S. Overexpression of miR-149-5p attenuates cerebral ischemia/reperfusion (I/R) injury by targeting Notch2. Neuromolecular Med. 2022;24(3):279–89.
42. Zheng S, Zhang P, Chen Y, Zheng S, Zheng L, Weng Z. Inhibition of Notch signaling attenuates schistosomiasis hepatic fibrosis via blocking macrophage M2 polarization. PLoS One. 2016;11(11):e0166808.
43. Lao Y, Li Y, Zhang P, Shao Q, Lin W, Qiu B, et al. Targeting endothelial Erk1/2-Akt axis as a regeneration strategy to bypass fibrosis during chronic liver injury in mice. Mol Ther. 2018;26(12):2779–97.
44. Lin RY, Wang JH, Lu XM, Zhou XT, Mantion G, Wen H, et al. Components of the mitogen-activated protein kinase cascade are activated in hepatic

cells by *Echinococcus multilocularis* metacestode. World J Gastroenterol. 2009;15(17):2116–24.
45. Zhou Z, Zhang R, Li X, Zhang W, Zhan Y, Lang Z, Tao Q, Yu J, Yu S, Yu Z, et al. Circular RNA cVIM promotes hepatic stellate cell activation in liver fibrosis via miR-122-5p/miR-9-5p-mediated TGF-beta signaling cascade. Commun Biol. 2024;7(1):113.
46. Gao H, Huo L, Mo X, Jiang B, Luo Y, Xu B, Li J, Ma X, Jing T, Feng Z, et al. Suppressive effect of pseudolaric acid B on Echinococcus multilocularis involving regulation of TGF-beta1 signaling in vitro and in vivo. Front Microbiol. 2022;13:1008274.
47. Kong M, Chen X, Lv F, Ren H, Fan Z, Qin H, et al. Serum response factor (SRF) promotes ROS generation and hepatic stellate cell activation by epigenetically stimulating NCF1/2 transcription. Redox Biol. 2019;26:101302.
48. Al-Hetty H, Ismaeel GL, Mohammad WT, Toama MA, Kandeel M, Saleh MM. Turki Jalil A: SRF/MRTF-A and liver cirrhosis: pathologic associations. J Dig Dis. 2022;23(11):614–9.
49. Zeng C, Wang YL, Xie C, Sang Y, Li TJ, Zhang M, et al. Identification of a novel TGF-beta-miR-122-fibronectin 1/serum response factor signaling cascade and its implication in hepatic fibrogenesis. Oncotarget. 2015;6(14):12224–33.

Publisher's Note